# Identification of the High Affinity $Mn^{2+}$ Binding Site of Bacteriophage λ Phosphoprotein Phosphatase: Effects of Metal Ligand Mutations on Electron Paramagnetic Resonance Spectra and Phosphatase Activities†

Daniel J. White, Nicholas J. Reiter, Robert A. Sikkink, Lian Yu, and Frank Rusnak*

*Section of Hematology Research and Department of Biochemistry and Molecular Biology, Mayo Clinic and Foundation, Rochester, Minnesota 55905*

*Received March 29, 2001; Revised Manuscript Received May 29, 2001*

ABSTRACT: Bacteriophage λ phosphoprotein phosphatase (λPP) has structural similarity to the mammalian Ser/Thr phosphoprotein phosphatases (PPPs) including the immunosuppressant drug target calcineurin. PPPs possess a conserved active site containing a dinuclear metal cluster, with metal ligands provided by a phosphoesterase motif plus two additional histidine residues at the C-terminus. Multiple sequence alignment of λPP with 28 eubacterial and archeal phosphoesterases identified active site residues from the phosphoesterase motif and in many cases 2 additional C-terminal His metal ligands. Most highly similar to λPP are *E. coli* PrpA and PrpB. Using the crystal structure of λPP [Voegtli, W. C., et al. (2000) *Biochemistry 39*, 15365−15374] as a structural and active site model for PPPs and related bacterial phosphoesterases, we have studied mutant forms of λPP reconstituted with $Mn^{2+}$ by electron paramagnetic resonance (EPR) spectroscopy, $Mn^{2+}$ binding analysis, and phosphatase kinetics. Analysis of $Mn^{2+}$-bound active site mutant λPP proteins shows that H22N, N75H, and H186N mutations decrease phosphatase activity but still allow mononuclear $Mn^{2+}$ and [$(Mn^{2+})_2$] binding. The high affinity $Mn^{2+}$ binding site is shown to consist of M2 site ligands H186 and Asn75, but not H22 from the M1 site which is ascribed as the lower affinity site.

Reversible phosphorylation of proteins is essential for the regulation of metabolism in all organisms and involves the transfer of the phosphoryl group ($-PO_3^{2-}$) from ATP to Ser, Thr, Tyr, Asp, and His residues of target proteins and enzymes. The enzymes catalyzing the addition of the phosphoryl group, protein kinases, include mitogen activated protein (MAP)[1] kinases (*1*−*3*), protein kinase C (*4*, *5*), cyclic AMP-dependent protein kinases (*6*−*8*), and two component histidine kinases prevalent in bacteria (*9*, *10*).

Phosphoprotein phosphatases reverse the action of protein kinases by removing the phosphoryl group from target proteins, ultimately transferring it to water to form orthophosphate as a product. The two major classes of eukaryotic protein phosphatases are the protein tyrosine phosphatases (PTPs) and protein serine/threonine phosphatases. These phosphatases are members of three structurally and mechanistically distinct gene families. The PTPs have in common a $HCX_5R$ sequence that constitutes the active site, and a catalytic mechanism involving the formation of a phosphoenzyme intermediate in which the phosphoryl group is transferred transiently to this conserved cysteine residue (*11*). The protein serine/threonine phosphatases, represented by the PPP and PPM protein phosphatase families, dephosphorylate phosphoserine and phosphothreonine residues and are metalloenzymes catalyzing direct phosphoryl group transfer to water (*12*−*14*). A subgroup of the PTPs, the dual-specificity phosphatases, are capable of dephosphorylating serine, threonine, and tyrosine phosphoamino acid residues (*15*−*18*).

Initially the serine/threonine phosphatases were divided into four classes depending upon their activities in the absence and presence of metal ions and inhibitors (*19*−*22*). The type 1 phosphatases, represented by protein phosphatase 1 (PP1), selectively dephosphorylate the β subunit of phosphorylase kinase and are inhibited by the phosphopeptide inhibitors 1 and 2. The class 2 phosphatases, which include protein phosphatases 2A (PP2A), 2B (PP2B or calcineurin), and 2C (PP2C), dephosphorylate the α subunit of phosphorylase kinase and are not inhibited by inhibitors 1 and 2. In addition, PP2B/calcineurin is inhibited by the immunosuppressant drugs cyclosporin A and FK506, while PP1 and PP2A are inhibited by nanomolar concentrations of okadaic acid. Protein phosphatase 2C (PP2C), a PPM class Ser/Thr phosphatase not related to the PPP class, is activated by $Mg^{2+}$ and unaffected by these macrolide inhibitors.

A more recent classification based on multiple sequence alignments places PP1, PP2A, and the catalytic subunit of calcineurin in the PPP family based on a conserved amino

† This work was supported by a grant from the National Institutes of Health (GM46865).

* To whom correspondence should be addressed at Mayo Clinic and Foundation, 200 First St. S.W., Rochester, MN 55905. Telephone: (507) 284-4743, Fax: (507) 284-8286, Email: rusnak@mayo.edu.

[1] Abbreviations: AA, atomic absorption spectroscopy; Amp, ampicillin; BSA, bovine serum albumin; DTT, dithiothreitol; EDTA, ethylenediaminetetraacetic acid; EPR, electron paramagnetic resonance; IPTG, isopropylthio-β-D-galactopyranoside; λPP, bacteriophage λ phosphoprotein phosphatase; MAP, mitogen activated protein; PP1, protein phosphatase 1; PP2A, protein phosphatase 2A; PP2B, calcineurin (protein phosphatase 2B, phosphatase-3); PP2C, protein phosphatase 2C; PPM, Ser/Thr phosphatase subfamily including PP2C homologues; PPP, Ser/Thr phosphatase subfamily including PP1, PP2A, calcineurin, and λPP; pNP, *p*-nitrophenol; pNPP, *p*-nitrophenyl phosphate; PTP, protein tyrosine phosphatase family; SDS, sodium dodecyl sulfate; WT, wild type.

10.1021/bi010637a CCC: $20.00 
Published on Web 07/06/2001

acid sequence termed the phosphoesterase motif, **D**X**H**$(X)_n$-G**D**XXD$(X)_m$G**N**HD/E (*23*−*25*). This primary sequence motif defines a $\beta\alpha\beta\alpha\beta$ secondary structural motif that forms a scaffold for a dinuclear metal ion active site cofactor, with the residues denoted in boldface serving as ligands to both metal ions. One of these metal ions, referred to as the M1 metal ion, is coordinated by a carboxylate and imidazole group from the first aspartate and histidine residue in the phosphoesterase motif noted above. The second metal ion, termed M2, is coordinated by the amido group of the conserved asparagine residue of the phosphoesterase motif and two histidine residues that are positioned beyond the C-terminus of this motif. A conserved aspartate residue coordinates to both M1 and M2 metal ions in a $\mu$-1,1 fashion. Metal binding studies indicate that of the two $Mn^{2+}$ ions that can be bound by $\lambda$PP, one is bound tighter than the other but the relationship of these to the structural M1 and M2 sites has not yet been revealed (*26*).

The phosphoprotein phosphatase from bacteriophage $\lambda$ ($\lambda$PP) shares amino acid sequence and biochemical similarity with the catalytic cores of calcineurin A, PP1, and PP2A within the phosphoesterase motif. Furthermore, PP1, $\lambda$PP, and calcineurin A share homology from a common ancestor as seen by comparison of their crystal structures (*27*−*31*). The folds of their catalytic core domains around the $\beta\alpha\beta\alpha\beta$ central motif are highly similar, and the active site protein metal ligands and their positions within the metal coordination sphere are almost identical.

Two recently identified phosphatases from *E. coli*, PrpA and PrpB, show high sequence similarity to $\lambda$PP and are involved in the sensing of misfolded proteins in the periplasm (*32*). Several cyanobacterial and archeal PPP type phosphatases also having sequence and likely structural similarity to calcineurin A, PP1, and $\lambda$PP have been identified recently by the bacterial genome sequencing projects. The specific roles of these bacterial PPPs in regulating metabolism are beginning to be characterized (*33*−*39*). Several PPP type homologues having various metabolic regulation functions have been identified in yeast (*40*). The biological role of $\lambda$PP in bacteriophage $\lambda$, if any, is unknown.

In this work we compare the phosphatase activities and spectroscopic (EPR) properties of wild-type and metal ligand mutants of $\lambda$PP to further characterize the biochemical properties and mechanistic roles of metal ligands to the dinuclear metal center. The identity of the high affinity $Mn^{2+}$ binding site is revealed and discussed in the context of metal activation and catalytic mechanism of the PPP family of metallophosphatases.

## EXPERIMENTAL PROCEDURES

*Materials.* Dithiothreitol, $MnCl_2$, *p*-nitrophenyl phosphate (pNPP), DEAE-Sephadex CL-6B, phenyl-Sepharose, Coomassie Brilliant Blue-R250, and BSA were purchased from Sigma (St. Loius, MO). YM10 Diaflo ultrafiltration membranes and centricon microconcentrators were purchased from Amicon, Inc. (Beverly, MA). NAP-25 gel filtration columns and phenyl-Sepharose resin were purchased from Pharmacia Biotech (Piscataway, NJ). The plasmid pT7-7 was obtained from Dr. Stanley Tabor (*41*). All chemicals were ACS grade, and glass still distilled water was used throughout. Bacterial growth media were purchased from Fisher Scientific Co. (Hanover Park, IL). Where required, buffers and glassware were treated with Chelex 100 resin (BioRad, Hercules, CA) to minimize metal contamination.

*Multiple Sequence Alignment of λPP-like Microbial Metallophosphoesterases.* Microbial metallophosphoesterase gene and/or amino acid sequences with high similarly to $\lambda$PP, as identified by BLAST searches (*42*, *43*), were retrieved from the National Center for Biotechnology Information (NCBI) finished and unfinished microbial genome database (http://www.ncbi.nlm.nih.gov:80/Microb_blast/unfinishedgenome-.html). Pairwise alignments of protein sequences were computed according to amino acid sequence similarity using CLUSTALX v1.8 (*44*−*46*), using the default gap opening and extension parameters (10 and 0.1, respectively) and the Gonnet 250 protein weight matrix. The output was trimmed at the N- and C-termini such that the termini of the alignment contain regions of high similarity. The alignment was performed again using the trimmed alignment as the input, improving the quality of the alignment by removing bias from dissimilar sequences at the N- and C-termini of the individual sequences. Polypeptides similar to $\lambda$PP were included from the following organisms (with corresponding three letter abbreviated names): Aac, *Actinobacillus actinomycetemcomitans*; Afu, *Archaeoglobus fulgidus*; Asp, *Anebena sp.*; Ban, *Bacillus anthracis*; Bps, *Burkholderia pseudomallei*; Bsu, *Bacillus subtilis*; Ccr, *Caulobacter crescentus*; Dra, *Deinococcus radiodurans*; Eco, *Escherichia coli*; Efa, *Enterococcus faecalis*; Fis, *Fervidobacterium islandicum*; Hin, *Haemophilus influenzae*; Kae, *Klebsiella aerogenes*; lam, bacteriophage $\lambda$; MaeU, *Microcystis aeruginosa* UTEX 2063; MaeP, *Microcystis aeruginosa* PCC 7820; Mth, *Methanosarcina thermophila*; Nco, *Nostoc commune*; Pab, *Pyrodictium abyssi*; Ppu, *Pseudomonas putida*; Sco, *Streptomyces coelicolor*; Spn, *Streptococcus pneumoniae*; Sso, *Sulfolobus solfataricus*; Ssp, *Synechocystis sp.*; Sty, *Salmonella typhimurium*; Tma, *Thermatogota maritima*.

*Site-Directed Mutagenesis of λPP.* Single and double point mutations encoding single amino acid substitutions in the $\lambda$PP gene were created using the MORPH II kit (Eppendorf-5 Prime, Inc., Boulder, CO). Oligonucleotide primers representing the $\lambda$PP coding strand sequence containing base substitutions to bring about the appropriate amino acid substitution were synthesized at the Mayo Clinic Molecular Biology Core Facility. The primers used in the mutagenesis reaction, with mutated codons underlined, are as follows:

H22N: 5′-TTGGCGATCTG<u>AAC</u>GGATGCTACA-3′

N75H: 5′-CTGTACGTGGA<u>CAC</u>CATGAGCAAA-3′

H92N: 5′-GAAACGTTAAT<u>AAC</u>TGGCTGCTTA-3′

H117N: 5′-AAGCTCTTGCC<u>AAT</u>AAAGCAGATG-3′

H139N: 5′-ATGTTATCTGC<u>AAC</u>GCCGATTATC-3′

H186N: 5′-TCATCTTTGGT<u>AAT</u>ACGCCAGCAG-3′

Mutant primers were phosphorylated using T4 polynucleotide kinase, and the mutagenesis reactions were carried out according to the manufacturer's instructions using the wild-type $\lambda$PP gene cloned into the plasmid T7-7 (*25*) as a template. Following the mutagenesis reaction, mutant plasmid DNA products were used to transform *E. coli* BMH 71-18

*mut*S cells, which are deficient in DNA mismatch repair. Plasmid DNA was isolated from at least six different colonies for each mutagenesis reaction using QIAprep Spin miniprep columns (QIAGEN Inc., Chatsworth, CA) according to the manufacturer's instructions. The entire λPP gene for each clone was sequenced at the Mayo Clinic Molecular Biology Core Facility to screen for plasmids with the desired mutation and lack of secondary mutations.

*Expression and Purification of WT and Mutant λPPs.* Plasmid pT7-7 derivatives carrying WT and mutant λPP DNA sequences were used to transform *E. coli* BL21(DE3) followed by plating onto LB agar plates containing 0.1 mg/mL ampicillin (Amp). A single colony from freshly transformed cells was used to inoculate 5 mL of LB broth containing 400 μg/mL Amp. These were grown at 37 °C to an optical density by light scattering at 600 nm of ≈1 in a Varian Cary 1 double beam spectrophotometer, after which a 100 μL aliquot was used to inoculate 100 mL of LB media containing 400 μg/mL Amp. These cultures were grown at 37 °C with shaking to an optical density at 600 nm of ≈1, and 10 mL was used to inoculate 1.5−2.0 L of 2×TY media containing 400 μg/mL Amp in 6 L Erlenmeyer flasks. These larger cultures were grown at 37 °C until the culture optical density at 600 nm reached 0.7−1.0, after which IPTG was added to a final concentration of 0.3 mM and the temperature was lowered to 23 °C. Approximately 12−20 h later, the cells were harvested by centrifugation at 1500*g*, washed once in 25 mM Tris-HCl, pH 7.8, 2 mM EDTA, 20% glycerol, recentrifuged, and resuspended at 1 mL per gram wet weight in the same buffer. Cells were lysed and homogenized in an ice-cooled Bead Beater (Biospec Products, Inc., Barlesville, OK) using 0.5 mm zirconia/silica beads. Ten 10 s bursts of vortexing were followed by 50 s pauses to prevent overheating. Alternatively, cells were lysed using an ice-cold French pressure cell operating at 15 000 psi at the orifice. All subsequent steps were performed at 4 °C. Cell lysates were centrifuged at 40000*g* for 2 h to pellet insoluble proteins and cell debris, and the supernatant was applied to a DEAE Sephadex CL-6B column equilibrated with 25 mM Tris-HCl, pH 7.8, 2 mM EDTA. The column was washed with 3 volumes of the same buffer; then λPP was eluted with 25 mM Tris-HCl, pH 7.8, 0.1 M NaCl, 2 mM EDTA. Fractions containing the majority of the phosphatase activity were pooled, NaCl was added to 0.5 M, and the solution was applied to a 100 mL column of phenyl-Sepharose equilibrated with 25 mM Tris-HCl, pH 7.8, 0.5 M NaCl. This column was washed with 3 volumes of the equilibration buffer and 3 volumes of 25 mM Tris-HCl, pH 7.8, and λPP was eluted from the column with 25 mM Tris-HCl, pH 7.8, 50% glycerol. Fractions were pooled according to their phosphatase activity and the purity of the enzyme as judged by SDS−PAGE (*25*, *26*). The purified apoenzyme was dialyzed twice against 4 L of 100 mM Tris-HCl, pH 7.8, 100 mM NaCl, 10% glycerol, and further concentrated to 19−60 mg/mL using YM-10 Diaflo ultrafiltration membranes and Centricon microconcentrators (Amicon, Beverly, MA) or Millipore (Bedford, MA) ultrafree concentrators. At this stage, the protein was frozen at −70 °C until further use.

*Protein Concentration Determination.* Concentrations of mixtures and cell extracts were determined using the Coomassie Plus Protein Assay Reagent (Pierce, Rockford, IL), using a BSA calibration curve. The concentration of the purified protein was also determined using $\epsilon_{280} = 41\,700$ $M^{-1}$ $cm^{-1}$ as described (*26*).

*Phosphatase Assays of Wild-Type and Mutant λ Protein Phosphatases.* Phosphatase activities of λPP proteins were measured in 100 mM Tris-HCl, pH 7.8, 100 mM NaCl, 10 mM pNPP, and 1 mM $MnCl_2$ by monitoring the increase in absorbance at 410 nm vs time, with $\epsilon_{410} = 14\,400$ $M^{-1}$ $cm^{-1}$ for pNP at pH 7.8. Kinetic parameters $k_{cat}$ and $K_M$ for pNPP were determined by a least-squares analysis of the velocity versus substrate concentration curve by fitting to the Michaelis−Menten equation, using substrate concentrations from 10 to 300 mM.

*Preparation of EPR Samples.* Samples of WT and mutant λPP containing $Mn^{2+}$ were prepared as described previously (*26*). In this procedure, λPP (1 mg/mL) was incubated overnight (10−16 h) at 4 °C in 25 mM Tris-HCl, pH 7.8, 0.1 M NaCl, 10% glycerol, and 1 mM $MnCl_2$. The samples were concentrated to at least 10 mg/mL, and excess $Mn^{2+}$ was removed by passage over a NAP-25 gel filtration column (Pharmacia) into the same buffer without $MnCl_2$. Fractions containing protein were concentrated to 250−500 μL, measured in triplicate for their protein concentration (16−60 mg/mL), and frozen in quartz EPR tubes by immersion in liquid nitrogen. Samples prepared using this procedure retain at least 1 equiv of tightly bound $Mn^{2+}$ but lose a variable fraction of the more loosely bound second equivalent of $Mn^{2+}$.

*$Mn^{2+}$ Titrations of WT and Mutant λPP EPR Samples.* EPR samples of mutant λPPs were titrated with substoichiometric quantities of $MnCl_2$ from a 20 mM $MnCl_2$, 0.1 M Tris-HCl, pH 7.8, 0.1 M NaCl, 10% glycerol stock solution followed by 10 min incubation and mixing at room temperature before freezing by immersion of the quartz EPR tube in liquid nitrogen. Following EPR analysis, the sample was thawed, a further aliquot of $MnCl_2$ was added and mixed for 10 min, and the sample was again refrozen. This was repeated until the last aliquot of $MnCl_2$ had been added. Previous studies have shown that repetitive freeze−thaw cycles do not appreciably damage the protein (*26*).

*EPR Spectroscopy.* EPR spectra were recorded using a Bruker ESP 300E spectrometer operating at X-band microwave frequency (9.46 GHz) with samples maintained at low temperature (3.3−208 K) using an Oxford Instruments ESR 900 continuous flow cryostat. Power saturation studies were performed at low temperatures (4−77 K) to determine conditions under which spectral features would not be saturated.

*Manganese Determination of EPR Samples by Atomic Absorption Spectroscopy.* Manganese analyses were performed by atomic absorption spectroscopy using a Perkin-Elmer 3100 atomic absorbance spectrometer on 50 μL aliquots of EPR samples diluted 1:100 in 25 mM Tris-HCl, pH 7.8, using this buffer as the blank. The instrument was calibrated using $MnCl_2$ solutions from 0.1 to 5 ppm Mn, prepared by dilutions from a 1000 ± 3 μg/mL standard solution of $MnCl_2$ in 2% $HNO_3$ (High-Purity Standards, Charleston, SC) by dilution in glass-distilled water. Buffer and water gave identical zero readings. The integration time was 3 s, and measurements were performed in triplicate on the same sample. A fit to the integrated peak intensity versus manganese concentration using a quadratic equation was

done for the standards and used to obtain manganese concentrations in each sample.

## RESULTS

*Identification of Putative Active Site Amino Acid Residues and Metal Ligands of Bacterial Metallophophoesterases by Multiple Sequence Analysis.* A set of 29 different eubacterial and archeal protein sequences were identified having significant similarity to $\lambda$PP by BLAST searches of the NCBI GenBank finished and unfinished microbial genome database. These include previously identified and putative phosphoprotein phosphatases (PRPs/PPPs) and diadenosine tetraphosphatases (ApaHs) (Figure 1). Only partial sequences for the genes from *Deinococcus radiodurans* PPP (missing C-terminus) and *Klebsiella aerogenes* ApaH (missing N-terminus) were retrieved due to incomplete sequence availability. These partial sequences and outlying sequences from *C. crecentus* and *N. commune* were not included in Figure 1, but are shown in the Supporting Information.

After multiple sequence alignment, several conserved amino acid residues were identified, including the previously described phosphoesterase motif, $DXH(X)_nDXXDR(X)_m$-RGHND/E (Figure 1) (*14*, *23*, *24*, *47*). The phosphoesterase motif in $\lambda$PP contains the metal ligands for the M1 site, D20, and H22, and the carboxamide ligand at the M2 site from the side chain of N75. In addition, the residue providing the carboxylate ligand bridging the M1 and M2 ions, D49, and a noncoordinating active site histidine ligand that may play a role as a general acid/base, H76, are absolutely conserved in the active site of all phosphoesterases of this homologous class.

Until recently, the identities of the remaining two histidine ligands at the M2 site were not well-defined since these residues fall outside the readily identifiable phosphoesterase motif. The multiple sequence alignment analysis presented here as well as spectroscopic data presented below indicate that H139 and H186 are the histidine ligands of the M2 site in $\lambda$PP, with homologous histidine residues in other members of the metallophophoesterase family shown in Figure 1. This result is verified by the recent crystal structure (*29*). H139 has been wrongly numbered as H140 in several articles (*14*, *48*), but analysis of the DNA sequence, and also the crystal structure, indicates the assignment of this histidine as residue 139 is correct as described by Barton (*24*). Other histidine residues in $\lambda$PP, H92, H117, and H155, do not fall into conserved regions in the multiple sequence alignment of Figure 1 and are therefore unlikely to be metal ligands at the M2 site.

Of the three conserved arginine residues in $\lambda$PP, R162 and R53 are the pair of requisite active site arginine residues, analogous to calcineurin residues R122 and R254 (*30*, *31*) and R96 and R221 in PP1 (*27*, *28*), which form a positively charged bridge/cap over the dinuclear metal containing active site and are important for catalysis (*47*, *48*). The guanidinium group of the third conserved arginine, R73, forms a strong 1.8 Å hydrogen bond with the side chain amide group of Q78. This interaction stabilizes the conformation of the C-terminal end of $\beta$-sheet 4 and the N-terminal end of $\alpha$-helix D, where metal ligand N75 and catalytically important H76 are located (*29*).

The $\lambda$PP sequence is very closely related to the sequences of the two protein phosphatases from *E. coli*, PrpA (104/214 residues, 48% identity, 64% similarity) and PrpB (98/214 residues, 45% identity, 63% similarity), and might be genetically related to them by horizontal gene transfer to or from a bacteriophage.

```
archeal (group 1)
PabPP1-arch3   GDTHG~GDYVDRG~RGNHES~RGLFC~FAPSLR~RAHEA
SsoPP1-arch1   GDTHG~GDYVDRE~RGNHES~KLKYP~FLPSIR~RGHEA
MthPP1-arch2   GDIHG~GDYVDRG~RGNHET~KEKAF~LTASRR~RGHTA

mixed bacterial A (group 2)
Scoppp         GDVHG~GDFTDRG~MGNHEL~LVHSD~TVRETI~RDEGG
Efappp         SDIHG~GDLNDRG~RGNHEE~FVHAG~WIREPF~FGHTI
Spnppp         GDVHG~GDLIDRG~SGNHEY~FVHAG~WLRKPF~FGHTP
Banppp         SDIHG~GDYVDRG~KGNHED~FVHAG~WIRNEF~FGHTE
MaePcy2        GDVHG~GDLIDRG~LGNHEY~LVHAG~WIRNEF~TGHTL
MaeUcy1        GDVHG~GDLIDRG~LGNHEY~LVHAG~WIRNEF~TGHTL
Sspppp         GDVHG~GDLIDRG~LGNHEQ~LVHAG~WIRDEF~TGHTI
Fisprp         GDIHG~GDYIDRG~RGNHEQ~FVHGG~WIREEF~FGHTP
Tmaprp         GDIHG~GDYVDRG~RGNHEE~FVHGG~WIRDEF~FGHTP

diadenosine tetraphosphatases (group 3)
AacapaH        GDLHG~GDLLARG~LANHDL~SPHLQ~YLDHRL~FGHWA
HinapaH        GDLQG~GDLVARG~LGNHDL~SPDLQ~YLDHRF~FGHWA
EcoapaH        GDVHG~GDLVARG~LGNHDL~SPELR~FPNGQL~FGHWA
StyapaH        GDVHG~GDLVARG~LGNHDL~SPELR~FPNGQL~FGHWA
KaeapaH        .....~GDLVARG~LGNHDL~SNELS~FPNGQL~FGHWA
BpsapaH        GDLQG~GDLVNRG~LGNHDL~SPDLK~TPEGAM~FGHWA

mixed bacterial B (group 4)
Ecoprpa        GDIHG~GDVIDRG~RGNHEQ~IAHAD~WSRSRL~FGHTP
lamprp         GDLHG~GDLVDRG~RGNHEQ~ICHAD~WNRERI~FGHTP
Ecoprpb        GDIHG~GDNIDRG~KGNHEA~IAHAD~WPVDRV~FGHMM
Ppuppp         GDIHG~GDLVDRG~QGNHEA~LLHAD~RQVCQW~VGHTP
Aspprpa        GDIHG~GDLVDRG~PGNHEN~VAHAG~GLPVRY~YGHTP
Afuprp         GDVHA~GDYADRG~RGNHES~ISRKE~YFFGKK~RAHEP
Hinppp         GDPHG~GDLQLTT~HGNHDS~LRHRT~CHEAPK~HGHHH

Conserved      DXH   DXXDR  RGNHE/D  H     R     GH

Phospho-       <--   -----  ---->/-
esterase motif
```

FIGURE 1: Segments from a multiple sequence alignment of bacterial PPPs and diadenosine tetraphosphatases (ApaHs). Predicted metal ligands are shown as boldface underlined characters, and additional active site residues are highlighted in boldface characters. The row labeled "Conserved" defines an extended phosphoesterase motif for microbial PPPs and ApaHs, with the standard phosphoesterase motif (*23*) underscored in the row labeled "Phospho-esterase motif". For $\lambda$PP, the residues in the motif are numbered as follows: D20, H22, D49, D52, R53, R73, N75, H76, E77, H139, R162, H186. The complete alignment, generated as described under Experimental Procedures, is available in the Supporting Information. Abbreviated sequence names are as follows (the first three characters denote the organism): Aac, *Actinobacillus actinomycetemcomitans*; Afu, *Archaeoglobus fulgidus*; Asp, *Anebena sp.*; Ban, *Bacillus anthracis*; Bps, *Burkholderia pseudomallei*; Bsu, *Bacillus subtilis*; Eco, *Escherichia coli*; Efa, *Enterococcus faecalis*; Fis, *Fervidobacterium islandicum*; Hin, *Haemophilus influenzae*; Kae, *Klebsiella aerogenes*; lam, *bacteriophage* $\lambda$; MaeU, *Microcystis aeruginosa* UTEX 2063; MaeP, *Microcystis aeruginosa* PCC 7820; Mth, *Methanosarcina thermophila*; Nco, *Nostoc commune*; Pab, *Pyrodictium abyssi*; Ppu, *Pseudomonas putida*; Sco, *Streptomyces coelicolor*; Spn, *Streptococcus pneumoniae*; Sso, *Sulfolobus solfataricus*; Ssp, *Synechocystis sp.*; Sty, *Salmonella typhimurium*; Tma, *Thermatogota maritima*. Terminal characters denote the type of phosphoesterase: PP1-arch*x*, archeal protein phosphatase-1; ppp and prp, bacterial phosphoprotein phosphatase; cyx, cyanobacterial phosphoprotein phosphatase; apaH, diadenosine tetraphosphatase. The neighbor-joining tree computed by CLUSTALX from the 29 microbial phosphatase sequences, used to calculate the final alignment, segregates the proteins according to 4 major groups: archeal, group 1; mixed bacterial A, group 2; diadenosine tetraphosphatases, group 3; mixed bacterial B, group 4.

*Phosphatase Activities of WT and Metal Ligand Mutant $\lambda$PP Proteins.* Table 1 shows kinetic parameters for $Mn^{2+}$-

Table 1: Kinetic Parameters for pNPP Hydrolysis by WT and Mutant λPPs

| mutation | sample | $k_{cat}$ ($s^{-1}$) | pNPP $K_M$ (mM) | $k_{cat}/K_M$ ($M^{-1}$ $s^{-1}$) | relative $k_{cat}/K_M$[a] |
|---|---|---|---|---|---|
| WT | WT λPP Prep #1 | $(1.1 \pm 0.02) \times 10^3$ | $11.4 \pm 0.8$ | $(9.6 \pm 2.5) \times 10^4$ | 1 |
| | WT λPP Prep #2 | $(5.0 \pm 0.5) \times 10^2$ | $10.3 \pm 0.7$ | $(4.9 \pm 1.4) \times 10^4$ | 0.51 |
| | WT λPP[b] | $(2.0 \pm 0.03) \times 10^3$ | $10.3 \pm 0.3$ | $(1.9 \pm 0.3) \times 10^5$ | 2.0 |
| | λPP(H92N) | $(4.9 \pm 0.50) \times 10^2$ | $16 \pm 1$ | $(3.1 \pm 0.8) \times 10^4$ | 0.32 |
| | λPP(H117N) | $(6.6 \pm 0.3) \times 10^2$ | $18 \pm 1$ | $(3.7 \pm 0.9) \times 10^4$ | 0.39 |
| M2 | λPP(N75H) | $3.1 \pm 0.3$ | $17 \pm 2$ | $(1.8 \pm 0.6) \times 10^2$ | $1.9 \times 10^{-3}$ |
| | λPP(H186N) | $(1.0 \pm 0.4) \times 10^{-1}$ | $90 \pm 10$ | $1.1 \pm 0.6$ | $1.1 \times 10^{-5}$ |
| M1 | λPP(H22N) | $5.0 \pm 0.1$ | $16 \pm 2$ | $(3.1 \pm 1.1) \times 10^2$ | $3.2 \times 10^{-3}$ |
| | λPP(H22N)[b] | $(5.0 \pm 0.0) \times 10^{-2}$ | $6.0 \pm 1.3$ | $8.3 \pm 3.9$ | $8.6 \times 10^{-5}$ |

[a] Relative $k_{cat}/K_M$ compared with wild-type λPP, preparation 1. [b] Values as determined by Zhuo et al. (*25*) and assayed under the following conditions: 100 mM Tris-HCl, pH 7.8, 1 mM $Mn^{2+}$, 10 mM DTT, and 20 mM pNPP (*47*).

dependent pNPP hydrolysis by WT and mutant λPP proteins. The entries in Table 1 are grouped according to the expected function and effect that mutagenesis might have on phosphatase activity. Thus, since H92 and H117 are not active site residues, mutagenesis to asparagine is not expected to affect formation of the [$(Mn^{2+})_2$] cluster or influence the kinetic parameters for phosphate ester hydrolysis, a result that is confirmed upon measurement. Mutant proteins H92N and H117N displayed activities only 2−3-fold lower than the activity of our best wild-type protein preparation. This is within the natural variability in activity found between different WT λPP preparations (*49*), verifying the hypothesis that H92 and H117 neither are metal ligands at the active site nor are required for efficient catalysis or structurally integrity.

The second group of mutants consists of proteins in which an active site metal ligand has been mutated. This group consists of H22N (M1 site), N75H (M2 site), and H186N (M2 site). Despite the fact that a [$(Mn^{2+})_2$] cluster is capable of being assembled in all the mutant λPP proteins (vide infra), all show significant decreases in catalytic efficiency. Of the mutant proteins prepared, H186N mutant showed the greatest loss of activity, 11 000 times less in terms of $k_{cat}$ relative to wild-type enzyme. The $K_M$ of this enzyme for pNPP is also increased 9-fold, resulting in a decrease in $k_{cat}/K_M$ of $10^5$. H186 therefore appears to be critical for enzymatic activation of the solvent nucleophile and/or substrate, and binding of the substrate. Most certainly H186 is involved in the reaction mechanism by virtue of being involved in $Mn^{2+}$ binding. Mutagenesis of H22 to asparagine and N75 to histidine leads to decreases in $k_{cat}$ values of more than 220- and 360-fold, respectively, without appreciably affecting pNPP $K_M$ values. The specific activity of our H22N preparation is higher than previously reported (*47*), perhaps indicating higher protein stability or integrity from this preparation. In terms of catalytic efficiency, the mutant proteins H22N and N75H are 200−300 times more active than H186N. H22 and N75 contribute a large activation effect on the reaction mechanism by enhancing the catalytic function of the two $Mn^{2+}$ ions, but are less critical than H186.

With similar reasoning, the H139N mutant protein should also have compromised phosphatase activity. Unfortunately, attempts to overexpress and purify to homogeneity recombinant λPP(H139N) protein were unsuccessful due to its tendency to form insoluble protein. Therefore, neither its activity nor its $Mn^{2+}$ binding properties could be assessed.

*Spectroscopic Evidence for the Identity of the High Affinity $Mn^{2+}$ Binding Site of λPP.* It has previously been shown that incubation of wild-type apo-λPP with $Mn^{2+}$ followed by concentration and desalting removes free and weakly bound $Mn^{2+}$. The result is <2 molar equiv of $Mn^{2+}$ bound at the active site and a mixture of both [$Mn^{2+}$]- and [$(Mn^{2+})_2$]-containing species, each of which gives rise to characteristic EPR spectra. These observations led to the discovery of two distinct $Mn^{2+}$ binding sites with discrete affinities: a high affinity site with a $K_{dM2}$ of ∼2 μM and a lower affinity site with a $K_{dM1}$ of ∼160 μM (*26*).

Table 2: Mn Stoichiometry of λPP EPR Samples[a]

| ligand[b] | mutant | [protein] (mM) | [$Mn^{2+}$] (mM) | [$Mn^{2+}$]/[protein] |
|---|---|---|---|---|
| N/A | WT | $1.32 \pm 0.18$ | $2.11 \pm 0.02$ | $1.6 \pm 0.2$ |
| N/A | H92N | $1.81 \pm 0.21$ | $2.82 \pm 0.02$ | $1.6 \pm 0.2$ |
| N/A | H117N | $1.34 \pm 0.19$ | $1.86 \pm 0.02$ | $1.4 \pm 0.2$ |
| M1 | H22N | $2.32 \pm 0.25$ | $3.48 \pm 0.02$ | $1.5 \pm 0.2$ |
| M2 | H186N | $0.67 \pm 0.09$ | $1.05 \pm 0.02$ | $1.6 \pm 0.2$ |
| M2 | N75N | $1.19 \pm 0.17$ | $1.96 \pm 0.02$ | $1.6 \pm 0.2$ |

[a] Protein and Mn concentration determinations were performed by UV absorbance and AA spectroscopies as described under Experimental Procedures. The ± values for manganese determination represent the standard deviation from the mean value of triplicate measurements. The error in protein concentration determination is estimated to be ±15%. [b] This column denotes whether the mutated ligand is in the coordination environment of the dinuclear metal center. M1 or M2 represents a mutated ligand bound directly to the M1 or M2 metal site, respectively. N/A represents a mutated residue that is not involved in binding $Mn^{2+}$.

We have constructed several semiconservative mutations of the active site metal ligands, replacing histidine ligands with asparagine, and vice versa, thereby interchanging metal ligation between nitrogen and oxygen atoms. These substitutions change the size and polarity of the amino acid residue as little as possible in an attempt to retain integrity and activity of the [$(Mn^{2+})_2$] cluster, but nevertheless modify the ligand field and ultimately affect the chemical properties of the metal ion. WT and metal ligand mutant λPP proteins were reconstituted with $Mn^{2+}$ using the incubation/desalting procedure. Manganese analyses (by atomic absorption spectroscopy, Table 2) and EPR spectroscopic studies (Figures 2 and 3) were carried out on WT and mutant proteins in order to determine the identity of the high affinity metal binding site.

Manganese analyses of $Mn^{2+}$-reconstituted WT and mutant $Mn^{2+}$-reconstituted λPP samples, performed by atomic absorption spectroscopy, confirm Mn stoichiometries less than 2, ranging from 1.4 to 1.6 mol of Mn/mol of protein (Table 2). The EPR spectra of these samples also indicated contributions of both mononuclear $Mn^{2+}$ and dinuclear

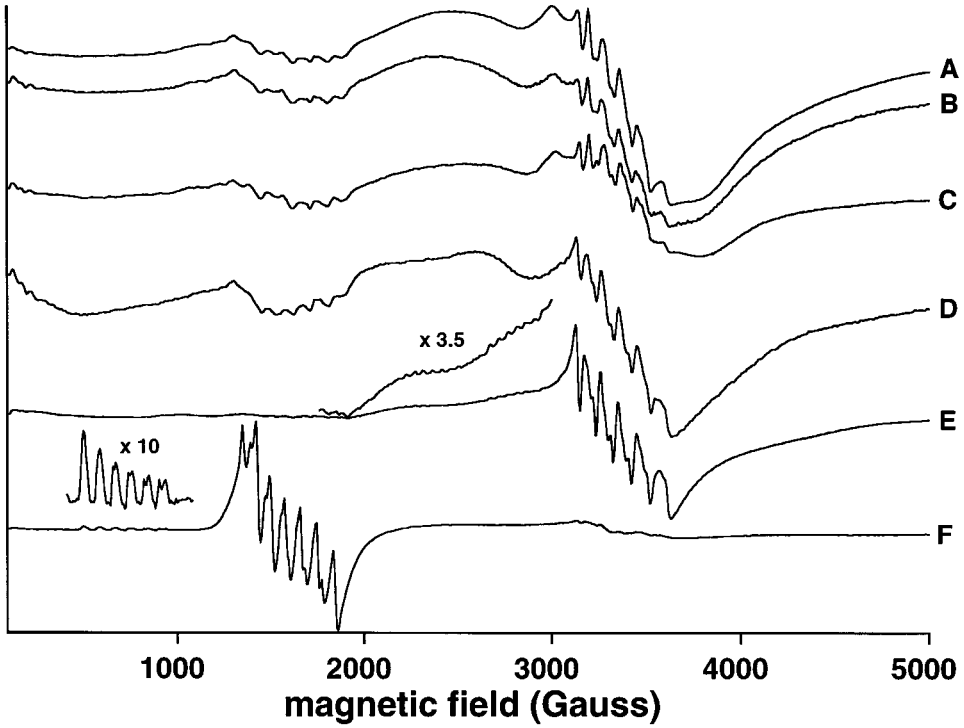


FIGURE 2: Low temperature EPR spectra of recombinant $\lambda$PPs WT (A), H117N (B), H92N (C), H22N (D), H186N (E), and N75H (F), following titration/reconstitution with $Mn^{2+}$. The H22N $\lambda$PP EPR spectrum (D) was collected from a sample prepared by titration with 1.5 equiv of $Mn^{2+}$ from a freshly prepared solution of 20 mM $MnCl_2$, 0.1 M Tris-HCl, pH 7.8, 0.1 M NaCl, 10% glycerol followed by 10 min incubation and mixing at room temperature. All other spectra were recorded on samples prepared as described by the incubation/desalting procedure described under Experimental Procedures. Table 1 shows the stoichiometries of $Mn^{2+}$ bound per protein for each sample. EPR spectrometer conditions were as follows: temperature, 3.3−4 K; microwave frequency, 9.46 GHz; microwave power, 0.5 mW; modulation amplitude, 2 G, at 100 kHz modulation frequency; 164 ms conversion time and time constant. All spectra are microwave power and gain normalized, and sample protein concentrations are comparable.

$[(Mn^{2+})_2]$ forms. At 4 K, the EPR spectrum is dominated by signals from the mononuclear $Mn^{2+}$ site. Characteristic EPR features of the mononuclear $Mn^{2+}$ site in WT $\lambda$PP are the following: (1) an intense, six-line $^{55}$Mn-hyperfine pattern centered near 3300 G ($g \approx 2$, $A = 88$ G); (2) a sharp feature at 3000 G that is not part of the six-line hyperfine pattern of the $g \approx 2$ resonance; (3) a broad and featureless peak from 2000 to 3000 G; (4) a hyperfine-split resonance from 1300 to 2100 G previously assigned to a "forbidden" $\Delta m_S = \pm 2$ transition ($g \approx 4.05$, $A = 87$ G); and (5) a weak very low field transition also exhibiting $^{55}$Mn hyperfine splitting (Figure 2A).

The 4 K EPR spectra of WT and mutant $\lambda$PP proteins shown in Figure 2 are of three types, depending upon whether a mutation was made at the M1 site, M2 site, or neither. Proteins in the first group, WT, H92N, and H117N, correspond to proteins that exhibit an EPR spectrum identical to the WT spectrum (Figure 2, spectra A, B, and C), indicating that the mononuclear $Mn^{2+}$ ion remaining tightly bound to these three enzymes is in an identical ligand field environment. These spectra provide evidence that His 92 and His 117 residues are not $Mn^{2+}$ ligands at the enzyme active site as predicted by multiple sequence alignments (Figure 1) and demonstrated recently in the X-ray structure of WT $\lambda$PP (*29*).

The second type of low temperature spectrum (Figure 2D) is represented by H22N, which has the histidine ligand at the M1 site mutated to asparagine. The EPR spectrum of H22N is quite similar to the WT spectrum, again indicating that the ligand environment for the tightly bound $Mn^{2+}$ ion in H22N is similar to WT $\lambda$PP. It is worth noting that there are subtle differences in the 4 K EPR spectra of H22N compared to WT $\lambda$PP, the most notable being the absence of the sharp resonance at 3000 G and an additional broad component from 2000 to 2500 G. These features probably represent signals originating from a dinuclear $[(Mn^{2+})_2]$ cluster. Additional differences in the EPR spectra of the $[(Mn^{2+})_2]$ cluster in WT and H22N become more apparent at higher temperatures (vide infra).

The third type of spectrum corresponds to mutations at the M2 site, represented by EPR spectra of N75H and H186N (Figure 2, spectra E and F, respectively). The EPR spectra of H75N and H186N proteins after $Mn^{2+}$ incubation/desalting treatment have dramatically different line shapes than the EPR spectrum of the wild-type protein. This indicates large differences in the ligand field of the mononuclear $Mn^{2+}$ ion bound at the high affinity site compared to WT. The spectrum of $Mn^{2+}$-reconstituted N75H at 4 K is characterized by an intense and sharp 6-line pattern centered at $g = 4.14$ ($A \approx 83$ G), and a weaker 6-line feature around $g = 10.9$. These resonances can be assigned to a mononuclear high spin $Mn^{2+}$ center due to the characteristic 6-line hyperfine patterns with $A \approx 90$ G (*26*, *50*). The $g = 10.9$ feature may alternatively arise from a $Mn^{3+}$ species (*51*). The 4 K EPR spectrum of $Mn^{2+}$-reconstituted H186N, in contrast, exhibits weaker low field (~1500 G) signals, but increased intensity in the $g = 2$ region compared to the WT enzyme. Also present are a pair of broad hyperfine split resonances seen as shoulders on the low field side of the intense $g = 2$ resonance, and an additional weak and broad shoulder at ~4500 G.

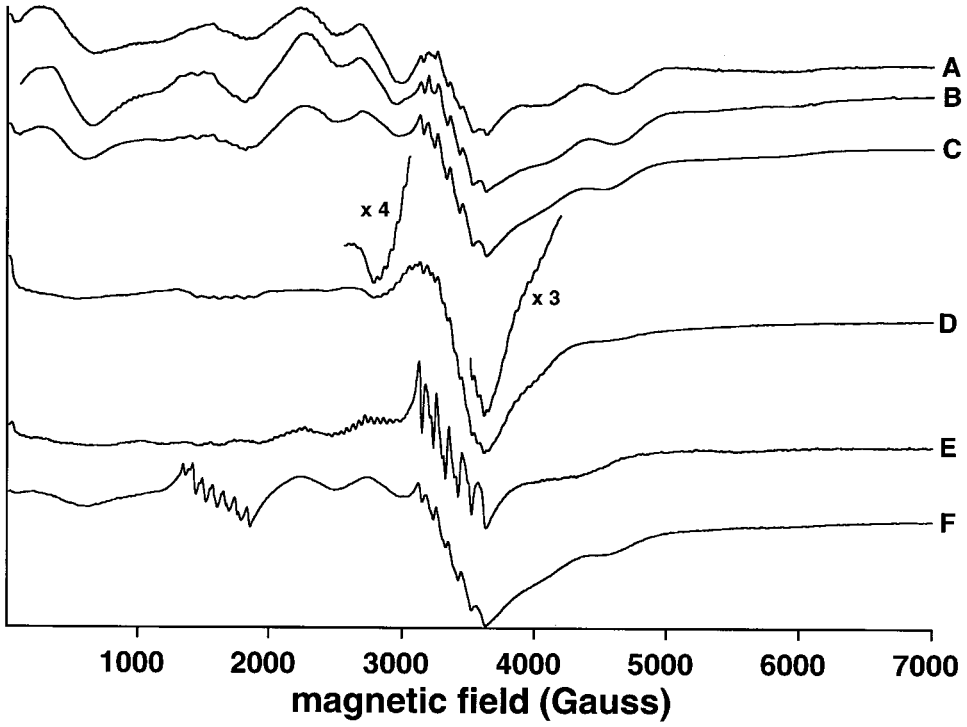


FIGURE 3: High temperature EPR spectra of WT and mutants. WT, 30 K, 20 mW (A); H92N, 30 K, 20 mW (B); H117N, 30 K, 20 mW (C); H22N, 30 K, 20 mW (D); H186N, 10 K, 0.5 mW (E); N75H, 30 K, 20 mW (F). EPR samples were prepared by the incubation/desalting procedure described under Experimental Procedures. EPR spectrometer conditions were as follows: microwave frequency, 9.46 GHz; modulation amplitude, 2 G, at 100 kHz modulation frequency; 164 ms conversion time and time constant. All spectra are microwave power and gain normalized, and sample protein concentrations are comparable.

A comparison of the EPR spectra in Figure 2 reveals that the M2 site is the high affinity $Mn^{2+}$ binding site since mutations of ligands to the metal ion in that site cause the biggest changes in the ligand field of the tightly bound $Mn^{2+}$ ion. Therefore, M2 becomes preferentially occupied over M1 by the first equivalent of $Mn^{2+}$. It is also worth noting that these semiconservative mutations in the active site do not result in loss of 4 K EPR spectra characteristic of mononuclear $Mn^{2+}$ bound to $\lambda$PP. Furthermore, from the kinetic data in Table 1, it is clear that the structural integrity of the M1 site is less critical for the catalytic efficiency of $\lambda$PP than that of the M2 site.

*High Temperature EPR Spectra of Weakly Coupled [$(Mn^{2+})_2$] Centers in WT and Mutant $\lambda$PPs.* High temperature EPR spectra of WT and metal ligand mutant $\lambda$PP samples reconstituted with $Mn^{2+}$ by the incubation/desalting procedure are shown in Figure 3. The signals from the mononuclear $Mn^{2+}$ site are less intense at these temperatures than they are at 4 K since they follow a Curie Law, $1/T$ temperature dependence. In contrast, since EPR spectra of the spin-coupled [$(Mn^{2+})_2$] cluster are contributed by excited state features, most are barely discernible at 4 K but increase in intensity as the temperature is raised. Thus, EPR resonances from the spin-coupled [$(Mn^{2+})_2$] cluster of WT $\lambda$PP become visible at 30 K (Figure 3A). The spectrum of WT $\lambda$PP shown in Figure 3A is essentially the same as previously observed (*26*) except that the features arising from the spin-coupled [$(Mn^{2+})_2$] species are more intense compared to residual signals from protein-bound mononuclear $Mn^{2+}$ and free $Mn^{2+}$. This fact is also reflected in a high Mn:$\lambda$PP stoichiometry for this sample, approaching 2:1 (Table 2). In accord with the EPR spectra at 4 K, the 30 K EPR spectra from $Mn^{2+}$-reconstituted mutant $\lambda$PP protein H92N (Figure 3B) and H117N (Figure 3C) are identical to the EPR spectrum of WT, confirming that neither H92 nor H117 participates in $Mn^{2+}$ coordination.

Although only minor differences were observed between the 4 K EPR spectra of WT and H22N protein (i.e., the spectra of the mononuclear form), the effect of the H22N mutation on the ligand field at the M1 site and on the [$(Mn^{2+})_2$] cluster is much more pronounced in the 30 K EPR spectrum (Figure 3D). In this mutant, the coordination environment of $Mn^{2+}$ in the M1 site is predicted to change as an amide ligand to the M1 site replaces the imidazole group of H22. The EPR spectrum of $Mn^{2+}$-reconstituted H22N $\lambda$PP at 30 K (Figure 3D) shows general similarity to the WT spectrum (Figure 3A), but also some clear differences. A set of overlapping resonances around the $g = 2$ (2800−4400 G) region of the spectrum all exhibit weak hyperfine structure with splitting of ~45 G, consistent with the presence of a spin-coupled [$(Mn^{2+})_2$] center. Hyperfine splitting of the shoulder around 4000 G can also be observed at 30 K (Figure 3E, inset). The intensities of the derivative-shaped resonance around 600 G, the two prominent resonances between 2000 and 3000 G, and the high field resonances around 4600 and 6000 G are all diminished compared to the WT enzyme.

In the H186N mutant, the coordination environment of $Mn^{2+}$ in the M2 site is predicted to change from $N_2O_4$ to $NO_5$ as an asparagine carboxamide ligand replaces the imidazole group of H186. At high temperature, this substitution results in an enhancement of signal intensity compared to WT, both in the $g = 2$ region as well as in the hyperfine lines from the [$(Mn^{2+})_2$] cluster. A shift of the broad high field resonances from the [$(Mn^{2+})_2$] center to a lower field is also observed. Comparing the 30 K EPR spectrum of WT

λPP (Figure 3A) to the 10 K EPR spectrum of H186N (Figure 3E), the most striking difference is the higher intensity around $g = 2$ compared to other resonances. This feature presumably reflects mononuclear $Mn^{2+}$ bound to the enzyme whose signal is still visible at 10 K, indicating incomplete formation of the dinuclear $Mn^{2+}$ cluster. The derivative-shaped resonance centered around 600 G in the WT spectrum is mostly absent in the H186N spectrum. Another clear difference between the WT and H186N high-temperature spectra is the shape and intensity of the resonances between 2000 and 3000 G, present in H186N as broad shoulders on the low field side of the intense $g = 2$ resonance. These features, even at 3.5 K, have resolved multiple hyperfine lines that reach maximal intensity around 10 K (Figure 2E, inset, and Figure 3E). The 11 lines centered at 2300 G have an average splitting of 45 G, and look similar in shape and splitting but more intense than the lines of the spin-coupled [$(Mn^{2+})_2$] cluster signal of the wild-type enzyme centered near the same magnetic field (*26*). The feature at 2800 G also exhibits many more than 6 lines expected for a mononuclear [$Mn^{2+}$] center, some of which are obscured by other resonances. The average hyperfine splitting of these lines, 48 G, is also less than expected for a mononuclear $Mn^{2+}$ ion. The presence of these 45−48 G split hyperfine lines indicates the presence of a spin-coupled [$(Mn^{2+})_2$] center in the H186N $Mn^{2+}$-reconstituted sample. Further, the positions of the broad high field resonances centered around ∼4500 and ∼5400 G are shifted downfield compared to the WT resonances. This shift of the resonances to lower field may be due to a change in the value of the zero field splitting parameters caused by a change in the Mn−Mn distance resulting from this histidine to asparagine mutation. Hyperfine splitting of the ∼4500 G resonance is observable with average hyperfine splitting, consistent with the resonance originating from a [$(Mn^{2+})_2$] center (data not shown).

Figure 3F shows a 30 K EPR spectrum of Mn-reconstituted N75H λPP mutant protein. In comparison to the 4 K spectrum of this sample (Figure 2F), several new features from a dinuclear $Mn^{2+}$ cluster appear. Interestingly, most of them have nearly the same shape, relative intensity, and position on the field axis as analogous signals of the [$(Mn^{2+})_2$] cluster in WT λPP (compare Figure 3F with Figure 3A). It thus appears that despite a mutation that clearly affects the ligand field of the $Mn^{2+}$ ion in the M2 site, the zero field splitting and spin coupling parameters of the coupled system appear to be quite similar to those for WT λPP.

*Titration of Mutant λPP Proteins with Substoichiometric Amounts of $Mn^{2+}$.* Samples of mutant λPP proteins H22N, H186N, and N75H were titrated with a series of substoichiometric equivalents of $Mn^{2+}$ to further characterize the order of binding of the two $Mn^{2+}$ ions. High temperature (10−30 K) EPR spectra during the $Mn^{2+}$ titration for these three mutants are shown in Figures 4, 5, and 6, respectively. Features attributed to a dinuclear $Mn^{2+}$ cluster, noted above in the discussion of the spectra of Figure 3, can be seen in EPR spectra of these Mn-titrated samples. Thus, hyperfine lines with a spacing of ≈45 G (Figure 4, 3000−4000 G) are observed in spectra of H22N when the $Mn^{2+}$ stoichiometry exceeds ≈1. Similar hyperfine lines attributed to the dinuclear $Mn^{2+}$ cluster of H186N are clearly visible in the 10 K spectra for Mn stoichiometries ≥0.78 (Figure 5). The appearance of EPR signals of the dinuclear $[Mn^{2+}]_2$ cluster at stoichiometries <1 suggests that the difference in dissociation constants for the two $Mn^{2+}$ of H186N may be smaller than the ca. 100-fold difference observed in the wild-

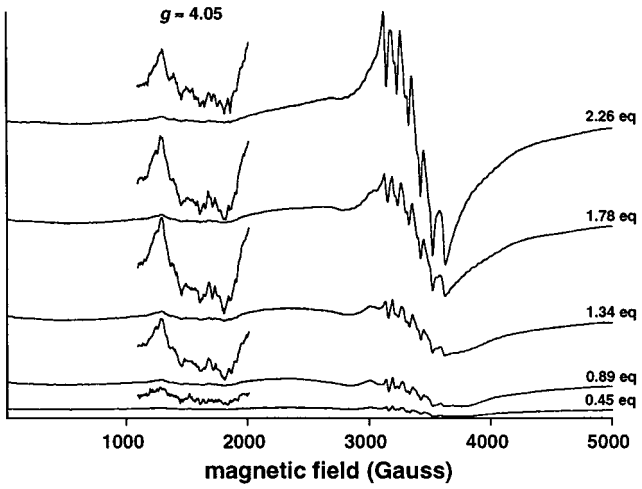


FIGURE 4: H22N $Mn^{2+}$ EPR titration at 30 K. Small aliquots of ∼0.5 equiv of $Mn^{2+}$ in 50 mM Tris-HCl, 100 mM NaCl, 10% glycerol buffer were added to the sample in the same buffer without $Mn^{2+}$ using a Hamilton microsyringe, mixed, and frozen by immersion of the sample tube in liquid nitrogen. After EPR analysis, the sample was thawed, and another ∼0.5 equiv of $Mn^{2+}$ was added, mixed, and then refrozen for further EPR analysis. This was repeated until ∼2−2.5 equiv of $Mn^{2+}$ had been added. After final EPR analysis, $Mn^{2+}$ content was measured by atomic absorption spectroscopy and λPP concentration was determined by UV absorbance at 280 nm to calculate accurate $Mn^{2+}$/λPP stoichiometries at each step. EPR spectrometer conditions were the following: microwave frequency, 9.46 GHz; microwave power, 20 mW; modulation amplitude, 2 G, at 100 kHz modulation frequency; 164 ms conversion time and time constant.

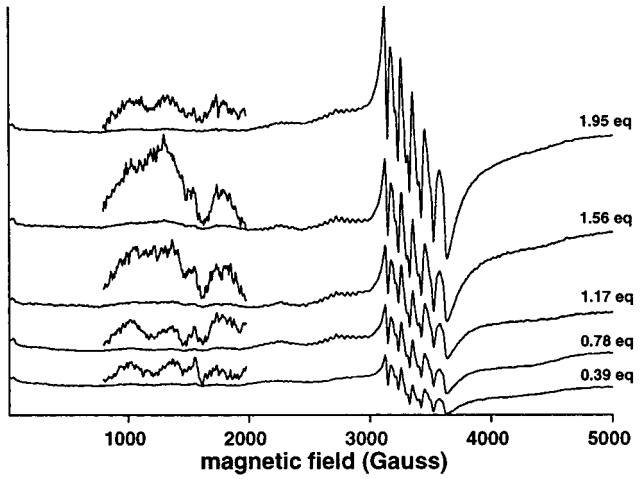


FIGURE 5: H186N $Mn^{2+}$ EPR titration at 10 K. Small aliquots of ∼0.5 equiv of $Mn^{2+}$ in 50 mM Tris-HCl, 100 mM NaCl, 10% glycerol buffer were added to the sample in the same buffer without $Mn^{2+}$ using a Hamilton microsyringe, mixed, and frozen by immersion of the sample tube in liquid nitrogen. After EPR analysis, the sample was thawed, and another ∼0.5 equiv of $Mn^{2+}$ was added, mixed, and then refrozen for further EPR analysis. This was repeated until ∼2−2.5 equiv of $Mn^{2+}$ had been added. After final EPR analysis, $Mn^{2+}$ content was measured by atomic absorption spectroscopy and λPP concentration determined by UV absorbance at 280 nm to calculate accurate $Mn^{2+}$/λPP stoichiometries at each step. EPR spectrometer conditions were as follows: microwave frequency, 9.46 GHz; microwave power, 0.5 mW; modulation amplitude, 2 G, at 100 kHz modulation frequency; 164 ms conversion time and time constant.

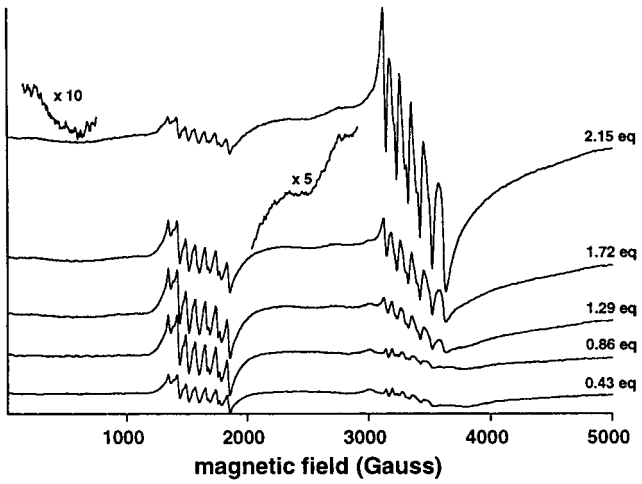


FIGURE 6: N75H $Mn^{2+}$ EPR titration at 30 K. Small aliquots of ~0.5 equiv of $Mn^{2+}$ in 50 mM Tris-HCl, 100 mM NaCl, 10% glycerol buffer were added to the sample in the same buffer without $Mn^{2+}$ using a Hamilton microsyringe, mixed, and frozen by immersion of the sample tube in liquid nitrogen. After EPR analysis, the sample was thawed, and another ~0.5 equiv of $Mn^{2+}$ was added, mixed, and then refrozen for further EPR analysis. This was repeated until ~2−2.5 equiv of $Mn^{2+}$ had been added. After final EPR analysis, $Mn^{2+}$ content was measured by atomic absorption spectroscopy and λPP concentration determined by UV absorbance at 280 nm to calculate accurate $Mn^{2+}$/λPP stoichiometries at each step. EPR spectrometer conditions were as follows: microwave frequency, 9.46 GHz; microwave power, 0.5 mW; modulation amplitude, 2 G, at 100 kHz modulation frequency; 164 ms conversion time and time constant.

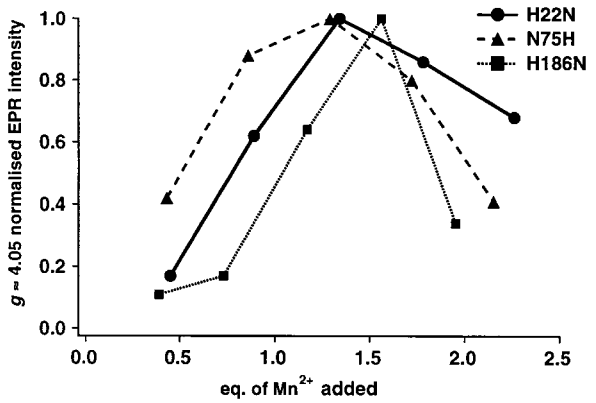


FIGURE 7: EPR intensity of the mononuclear [$Mn^{2+}$] site $g \approx 4.05$ feature vs equivalents of $Mn^{2+}$ added to mutant λPP proteins H22N, H186N, and N75H. EPR intensity was measured from peak to trough and then normalized by division with the highest EPR intensity at $g \approx 4.05$ for that sample.

type enzyme (*26*). The two prominent features between 2000 and 3000 G associated with the dinuclear $Mn^{2+}$ cluster in N75H are also present, albeit appearing significantly less intense relative to other signals in the spectrum, and then so are only really obvious when the Mn stoichiometry approaches or exceeds 2 equiv. In all three titrations (Figures 4, 5, and 6), the intensity of the forbidden $\Delta m_s = \pm 2$ signal around 1500−2000 G increases as the Mn stoichiometry increases toward 1 equiv, but then subsequently declines as the Mn stoichiometry approaches 2 equiv (Figure 7). In the cases of all three metal ligand mutants, this seems consistent with the high affinity M2 site being filled first. However, it is puzzling that there is no further increase in intensity between 1 and 2 equiv of $Mn^{2+}$ in the hyperfine split signals of the spin-coupled [$(Mn^{2+})_2$] species on the low field shoulder of the intense $g = 2$ resonance in the H186N titration spectra. Part of the difficulty in quantifying the intensities of these and other features of the [$(Mn^{2+})_2$] cluster (most notable for H186N, Figure 5) relates to the fact that these spectra are dominated by signals from both the mononuclear $Mn^{2+}$ ion as well as free $Mn^{2+}$, both which partially overlap resonances from the [$(Mn^{2+})_2$] center. This could not be avoided since samples prepared by the titration method have more of these species present (relative to the [$(Mn^{2+})_2$] center) compared to samples prepared by the incubation/desalting method.

## DISCUSSION

In this study, active site mutants of λPP have been generated with the goal of addressing biochemical aspects of the metallophosphoesterase family of enzymes that includes not only λPP and numerous similar eubacterial and archeal phosphoesterases, but also some important eukaryotic homologues such as PP1, PP2A, and the calcineurin A catalytic subunit. Three-dimensional structure determination by X-ray crystallography of PP1, calcineurin, and recently λPP has revealed that these enzymes are structural homologues, sharing a common three-dimensional fold in the catalytic core domains (*27*−*31*). Most importantly, all three enzymes have active sites consisting of an identical constellation of amino acid residues that bind two metal ions, M1 and M2, as a dinuclear metal center. This allows us to confidently use λPP as a model system to describe and explain the chemistry and phosphoesterase activities of the active sites in more complex eukaryotic Ser/Thr phosphatases.

In a previous study investigating $Mn^{2+}$ binding to λPP, we have shown that the two $Mn^{2+}$ binding sites, collectively forming an active site [$(Mn^{2+})_2$] cluster, each have distinct affinities for $Mn^{2+}$ (*26*). Thus, WT λPP reconstituted with $Mn^{2+}$ by a procedure that involves removal of free and weakly bound $Mn^{2+}$ by gel filtration chromatography resulted in ≈1 equiv of $Mn^{2+}$ remaining bound to the enzyme. Selective population of a single $Mn^{2+}$ site rather than cooperative assembly of the [$(Mn^{2+})_2$] cluster was also observed during stepwise titration of the apoprotein with $Mn^{2+}$ (*26*). Similar results were obtained in this study, with both WT and metal ligand mutant proteins retaining ≈1.5 equiv of $Mn^{2+}$ following gel filtration chromatography. The latter result is important as it indicates that mutating selected active site metal ligands, from His to Asn, or from Asn to His, does not disrupt the ability of the protein to bind either one or both $Mn^{2+}$ ions of the [$(Mn^{2+})_2$] center. This result was confirmed by EPR analysis that showed features attributable to both mononuclear and spin-coupled dinuclear $Mn^{2+}$ centers. Although the tightly bound $Mn^{2+}$ ion in WT λPP exhibited EPR signals characteristic of a mononuclear high-spin $Mn^{2+}$ ion in an asymmetric ligand field, the relationship between the structural M1/M2 sites and the biochemically distiguishable high and low affinity sites was previously not evident. By comparing and contrasting the EPR properties of enzymes with mutations of either M1 or M2 ligands, we have determined that the high affinity $Mn^{2+}$ binding site in λPP is the M2 site. The ligands making up the M2 site consist of two histidine residues, H139 and H186, and a carboxamide from N75. In addition, a carboxylate from

Scheme 1: Theoretical Kinetic Catalytic Mechanism for Sequential $Mn^{2+}$ Binding and Substrate Turnover by PPP Type Phosphatases[a]

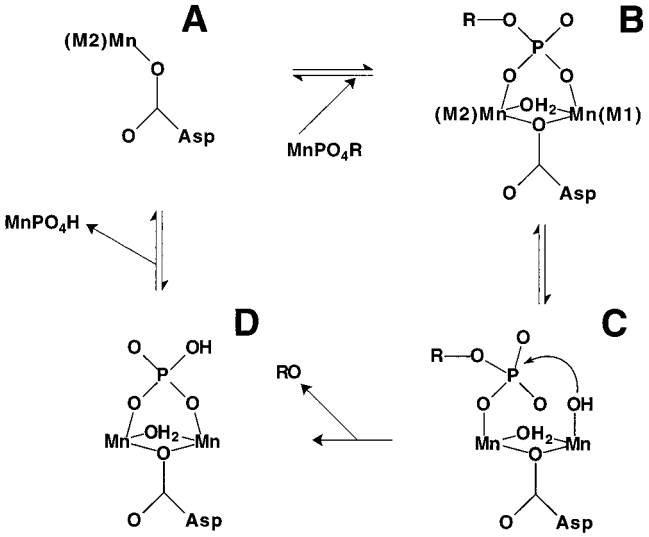


[a]The M2 site has high affinity for $Mn^{2+}$ and is likely to be fully occupied by $Mn^{2+}$ throughout the reaction. In contrast, the M1 site has lower affinity for $Mn^{2+}$, such that it is unlikely to be occupied by $Mn^{2+}$ in the resting enzyme under physiological conditions. Species A shows the resting enzyme, with metal ligand residues other than the bridging Asp omitted for clarity. Species A binds the Mn−substrate complex, bringing $Mn^{2+}$ to the M1 site. Concomitant binding of the substrate phosphoryl group to M2 results in a substrate-bridged complex, depicted as species B. Next, the phosphoryl group of substrate is transferred to the M2 site, resulting in an M2 terminal coordination mode analogous to the M2 terminally coordinated mode as seen in the crystal structure of $\lambda$PP (*29*), depicted as species C. P−O bond cleavage results when a solvent nucleophile bound terminally to M1 attacks the phosphorus atom, releasing the Ser/Thr product leaving group, and forming a bridged product complex, species D. This species is identical to the product-inhibited states of PP1 and calcineurin, as seen in crystal structures of anion-inhibited forms of these enzymes (*28*, *30*). The reaction cycle is complete following orthophosphate dissociation along with the M1 metal ion.

D49 and a solvent molecule bridge the M2 and M1 ions. These same amino acid side chains are likely to coordinate the mononuclear $Mn^{2+}$ ion in the M2 site in the absence of the second $Mn^{2+}$ ion (M1).

The biochemical significance of two $Mn^{2+}$ sites with distinct affinities indicates that, under physiological conditions, $Mn^{2+}$ may never occupy the lower affinity site of the resting enzyme since the concentration of free $Mn^{2+}$ in the cell needs to approach $K_{dM1}$ ($\sim$160 $\mu$M) for binding the more weakly bound $Mn^{2+}$ ion. One possibility is that the second $Mn^{2+}$ ion may enter the enzyme complexed to the phosphoryl group of substrate. Indeed the artificial substrate pNPP readily forms a complex with $Mn^{2+}$ with a $K_A$ of 74 $M^{-1}$. Although pNPP is not the physiological substrate, the phosphate groups of phosphoserine- and phosphothreonine-containing peptides may well complex metal ions such as $Mn^{2+}$. Thus, one possible kinetic mechanism is as follows (Scheme 1). The resting enzyme, starting with one $Mn^{2+}$ bound at the high affinity M2 site, binds the phosphorylated substrate complexed with a divalent metal ion. A consequence of this is that the dinuclear metal center only forms in the presence of substrate, with the second metal ion filling the M1 site upon formation of the quaternary $\lambda$PP·M2·pNPP·M1 complex, most likely in a bridged conformation as shown in Scheme 1B. This mechanism raises an important issue with regard to the formation of the quaternary complex. Other studies have proposed that the initial substrate complex has the substrate terminally coordinated to the M2 ion via one of the phosphate oxygen atoms. The evidence for this model comes from a study investigating phosphate binding to purple acid phosphatase. In that study, the authors proposed rapid binding of phosphate to the M2 ion followed by a slower isomerization step leading to a bridging mode in which two oxygen atoms of phosphate coordinate both M1 and M2 ions (*52*). The recent X-ray structure of $\lambda$PP complexed with sulfate in two coordination modes (terminal to M2 and triply bridged) also suggests that the quaternary complex has the substrate interacting with the M2 ion via an oxygen atom of the phosphoryl group, prior to P−O bond cleavage. If the M2 site becomes preferentially occupied over the M1 site as indicated in this study, it is difficult to reconcile substrate binding initially to the M2 $Mn^{2+}$ ion in a terminal fashion without also at least some interaction with the $Mn^{2+}$ ion in the M1 site. If substrate binds to the mononuclear $Mn^{2+}$ form of $\lambda$PP as a complex with $Mn^{2+}$, the initial substrate complex would instead have the substrate phosphoryl group bridging the M1 and M2 metal ions in a configuration similar to that seen in the product-inhibited complexes of PP1 and calcineurin (Scheme 1B) (*30*, *31*, *53*), or the tridentate coordination mode of sulfate bound to $\lambda$PP (*29*). This complex could then rearrange to the M2 terminal coordination mode after some ligand rearrangements involving transfer of the substrate phosphoryl group to M2, an intermediate that might actually represent a species one step closer to the transition state, rather than an earlier intermediate as previously envisioned (*29*). Obviously, additional work needs to be done to resolve these and other issues regarding the chemical steps in catalysis.

Another interesting finding of the present study was the observation that substitution of metal ligands brought about a change in the metal cluster ligand field that affected enzyme activity in the mutant enzymes. Mutagenesis of both M1 and M2 metal ligands brought about a $10^3-10^5$-fold decrease in phosphatase activity. EPR studies and Mn stoichiometry determinations clearly demonstrate that these mutations do not prevent the formation of a $[(Mn^{2+})_2]$ center, therefore ruling out the possibility that the loss of activity is due to the inability to form a $[(Mn^{2+})_2]$ center. Rather, mutagenesis appears to have affected the chemical properties of the $[(Mn^{2+})_2]$ center, making it a poorer catalyst for phosphate ester hydrolysis. Possible explanations include a change in Lewis acidity of one or both metal ions that affects the ability to activate the nucleophilic water molecule or phorphoryl group of substrate. Alternatively, the spacing of the two metal ions or positioning of key groups in the active site may have been affected, resulting in suboptimal alignment of substrate in the transition state. These issues might be resolved by determining the three-dimensional structures of some of these mutants.

The neighbor-joining tree from the alignment of 29 microbial phophoesterases has 4 main branches. These branches do not fully segregate the archea from the eubacteria. It is difficult to gain detailed phylogenetic information, as the sequences are relatively short and dissimilar. However, it is clear that $\lambda$PP is most closely similar to the two *E. coli* protein phosphatases, falling between them on a discrete branch of the neighbor-joining tree. Consequently, it is likely

that bacteriophage λ acquired the λPP gene as a copy of the *prpA* or *prpB* periplasmic protein misfolding sensor genes by horizontal gene transfer from a strain of enteric eubacterium closely related to the *E. coli* clone(s) used for genomic sequencing.

Diadenosine 5′,5‴-P1,P4-tetraphosphate (Ap4A) controls the timing of cell division in *E. coli*. Levels of Ap4A are controlled by diadenosine tetraphosphatase, encoded by *apaH*. The ApaH sequences in Figure 1 lack the first C-terminal His residue (apart from the *A. actinomycetemcommitans* sequence), but good metal ligand residues, Asp or Glu, occupy this position. This difference in metal ligation at the M2 site between ApaH and λPP might mirror some difference in the nature of the phosphodiesterase reaction catalyzed by ApaH compared to the phosphomonoesterase reaction catalyzed by λPP. The *E. coli* phosphoesterases PrpA and ApaH share not only similar sequences and active site structure, but also roles in regulation of cellular processes.

We can also conclude from the alignment presented in Figure 1 that in many cases when a positively charged or polar group is present at the same position as R73, a polar or negatively charged group is present at the same position as Q78. It can also be seen that if one of these positions is occupied by a hydrophobic residue then the other position is often filled by another hydrophobic residue, as in the cases of the ApaH enzymes where positions equivalent to 73 and 78 in λPP are occupied by Leu residues. Mutations of R73 cause a ∼20-fold decrease in phosphatase activity probably by disruption of the structure of the protein in this critical region, not due to removal of an interaction with product phosphate as previously described (*47*).

The conserved residues D52 and D77 are similarly important in stabilizing the conformation of the active site. D52 may form a H-bonded bridge between the pyrrole nitrogen of W100 and the imidazole side chain of active site H76, adding to the conformational stability of this catalytically important His residue. The carboxylate side chain of D77 hydrogen bonds to backbone amide protons of the essential bridging metal ligand residue D49 and the adjacent residue L50, anchoring the C-terminal end of β-sheet 4 to α-helix C. Residues D202 and S/T203 are also well conserved in some of the enteric bacterial ApaH and PPP sequences, but not in *H. influenzae* or the cyanobacteria. In the structure of λPP, D202 interacts with a solvent ligand to M1, which is probably not the nucleophile of the phosphoesterase reaction as it is too distant from the substrate modeled into the active site (5.6 Å). However, being located in the substrate binding groove, D202 could be involved in recognition of substrates containing positively charged surface residues (*29*).

With the data presented in this paper, along with the recent λPP crystal structure and further mechanistic data, we are extending our understanding of the catalytic mechanism(s) of dinuclear metal cluster containing hydrolases. We continue to further our knowledge of why the ligand field created for the metal cluster in these hydrolytic enzymes favors hydrolytic chemistry over redox reactions, as seen in enzymes of similar active site structure, such as Mn catalases (*54*−*57*). This information might lead toward the rational design of better inhibitors of this class of regulatory phosphoesterases.

## SUPPORTING INFORMATION AVAILABLE

Multiple sequence alignment of bacterial phosphoesterases computed using CLUSTAL X, displayed in GCG MSF format (10 pages). This material is available free of charge via the Internet at http://pubs.acs.org.

## REFERENCES


1. Meskiene, I., and Hirt, H. (2000) *Plant Mol. Biol. 42*, 791−806.
2. Camps, M., Nichols, A., and Arkinstall, S. (2000) *FASEB J. 14*, 6−16.
3. Cobb, M. H. (1999) *Prog. Biophys. Mol. Biol. 71*, 479−500.
4. Black, J. D. (2000) *Front. Biosci. 5*, D406−D423.
5. Newton, A. C., and Johnson, J. E. (1998) *Biochim. Biophys. Acta 1376*, 155−172.
6. Taylor, S. S., Buechler, J. A., and Yonemoto, W. (1990) *Annu. Rev. Biochem. 59*, 971−1005.
7. Taylor, S. S., Radzio-Andzelm, E., Knighton, D. R., Ten Eyck, L. F., Sowadski, J. M., Herberg, F. W., Yonemoto, W., and Zheng, J. (1993) *Receptor 3*, 165−172.
8. Taylor, S. S., Radzio-Andzelm, E., Madhusudan, Cheng, X., Ten Eyck, L., and Narayana, N. (1999) *Pharmacol. Ther. 82*, 133−141.
9. Falke, J. J., Bass, R. B., Butler, S. L., Chervitz, S. A., and Danielson, M. A. (1997) *Annu. Rev. Cell Dev. Biol. 13*, 457−512.
10. Hoch, J. A. (2000) *Curr. Opin. Microbiol. 3*, 165−170.
11. Denu, J. M., and Dixon, J. E. (1998) *Curr. Opin. Chem. Biol. 2*, 633−641.
12. Barford, D., Das, A. K., and Egloff, M.-P. (1998) *Annu. Rev. Biophys. Biomol. Struct. 27*, 133−164.
13. Rusnak, F. (2000) *Met. Ions Biol. Syst. 37*, 305−343.
14. Lohse, D. L., Denu, J. M., and Dixon, J. E. (1995) *Structure 3*, 987−990.
15. Keyse, S. M. (2000) *Curr. Opin. Cell Biol. 12*, 186−192.
16. Haneda, M., Sugimoto, T., and Kikkawa, R. (1999) *Eur. J. Pharmacol. 365*, 1−7.
17. Zhang, M., Stauffacher, C. V., Lin, D., and Van Etten, R. L. (1998) *J. Biol. Chem. 273*, 21714−21720.
18. Wang, S. S., Tabernero, L., Zhang, M., Harms, E., Van Etten, R. L., and Stauffacher, C. V. (2000) *Biochemistry 39*, 1903−1914.
19. Ingebritsen, T. S., and Cohen, P. (1983) *Science 221*, 331−338.
20. Cohen, P. (1989) *Annu. Rev. Biochem. 58*, 453−508.
21. Shenolikar, S., and Nairn, A. C. (1991) *Adv. Second Messenger Phosphoprotein Res. 23*, 3−121.
22. Rusnak, F., Yu, L., and Mertz, P. (1996) *J. Biol. Inorg. Chem. 1*, 388−396.
23. Koonin, E. V. (1994) *Protein Sci. 3*, 356−358.
24. Barton, G. J., Cohen, P. T. W., and Barford, D. (1994) *Eur. J. Biochem. 220*, 225−237.
25. Zhuo, S., Clemens, J. C., Hakes, D. J., Barford, D., and Dixon, J. E. (1993) *J. Biol. Chem. 268*, 17754−17761.
26. Rusnak, F., Yu, L., Todorovic, S., and Mertz, P. (1999) *Biochemistry 38*, 6943−6952.
27. Goldberg, J., Huang, H.-B., Kwon, Y.-G., Greengard, P., Nairn, A. C., and Kuriyan, J. (1995) *Nature 376*, 745−753.
28. Egloff, M.-P., Cohen, P. T. W., Reinemer, P., and Barford, D. (1995) *J. Mol. Biol. 254*, 942−959.
29. Voegtli, W. C., White, D. J., Reiter, N. J., Rusnak, F., and Rosenzweig, A. C. (2000) *Biochemistry 39*, 15365−15374.
30. Griffith, J. P., Kim, J. L., Kim, E. E., Sintchak, M. D., Thomson, J. A., Fitzgibbon, M. J., Fleming, M. A., Caron, P. R., Hsiao, K., and Navia, M. A. (1995) *Cell 82*, 507−522.
31. Kissinger, C. R., Parge, H. E., Knighton, D. R., Lewis, C. T., Pelletier, L. A., Tempczyk, A., Kalish, V. J., Tucker, K. D., Showalter, R. E., Moomaw, E. W., Gastinel, L. N., Habuka, N., Chen, X. H., Maldonado, F., Barker, J. E., Bacquet, R., and Villafranca, J. E. (1995) *Nature 378*, 641−644.
32. Missiakas, D., and Raina, S. (1997) *EMBO J. 16*, 1670−1685.

33. Mai, B., Frey, G., Swanson, R. V., Mathur, E. J., and Stetter, K. O. (1998) *J. Bacteriol. 180*, 4030−4035.
34. Shi, L., Carmichael, W. W., and Kennelly, P. J. (1999) *J. Biol. Chem. 274*, 10039−10046.
35. Solow, B., Young, J. C., and Kennelly, P. J. (1997) *J. Bacteriol. 179*, 5072−5075.
36. Leng, J., Cameron, A. J. M., Buckel, S., and Kennelly, P. J. (1995) *J. Bacteriol. 177*, 6510−6517.
37. Potts, M., Sun, H., Mockaitis, K., Kennelly, P. J., Reed, D., and Tonks, N. K. (1993) *J. Biol. Chem. 268*, 7632−7635.
38. McCartney, B., Howell, L. D., Kennelly, P. J., and Potts, M. (1997) *J. Bacteriol. 179*, 2314−2318.
39. Zhang, C.-C., Friry, A., and Peng, L. (1998) *J. Bacteriol. 180*, 2616−2622.
40. Stark, M. J. R. (1996) *Yeast 12*, 1647−1675.
41. Tabor, S., and Richardson, C. C. (1985) *Proc. Natl. Acad. Sci. U.S.A. 82*, 1074−1078.
42. Altschul, S. F., Gish, W., Miller, W., Myers, E. W., and Lipman, D. J. (1990) *J. Mol. Biol. 215*, 403−410.
43. Altschul, S. F., Madden, T. L., Schaffer, A. A., Zhang, J., Zhang, Z., Miller, W., and Lipman, D. J. (1997) *Nucleic Acids Res. 25*, 3389−3402.
44. Thompson, J. D., Gibson, T. J., Plewniak, F., Jeanmougin, F., and Higgins, D. G. (1997) *Nucleic Acids Res. 25*, 4876−4882.
45. Higgins, D. G., and Sharp, P. M. (1988) *Gene 73*, 237−244.
46. Higgins, D. G., and Sharp, P. M. (1989) *Comput. Appl. Biosci. 5*, 151−153.
47. Zhuo, S., Clemens, J. C., Stone, R. L., and Dixon, J. E. (1994) *J. Biol. Chem. 269*, 26234−26238.
48. Ansai, T., Dupuy, L. C., and Barik, S. (1996) *J. Biol. Chem. 271*, 24401−24407.
49. Mertz, P., Yu, L., Sikkink, R., and Rusnak, F. (1997) *J. Biol. Chem. 272*, 21296−21302.
50. Reed, G. H., and Markham, G. D. (1984) *Biol. Magn. Reson. 6*, 73−142.
51. Campbell, K. A., Yikilmaz, E., Grant, C. V., Gregor, W., Miller, A.-F., and Britt, R. D. (1999) *J. Am. Chem. Soc. 121*, 4714−4715.
52. Aquino, M. A. S., Lim, J. S., and Sykes, A. G. (1994) *J. Chem. Soc., Dalton Trans*., 429−436.
53. Egloff, M.-P., Johnson, D. F., Moorhead, G., Cohen, P. T. W., Cohen, P., and Barford, D. (1997) *EMBO J. 16*, 1876−1887.
54. Khangulov, S., Sivaraja, M., Barynin, V. V., and Dismukes, G. C. (1993) *Biochemistry 32*, 4912−4924.
55. Khangulov, S. V., Pessiki, P. J., Barynin, V. V., Ash, D. E., and Dismukes, G. C. (1995) *Biochemistry 34*, 2015−2025.
56. Dismukes, G. C. (1996) *Chem. Rev. 96*, 2909−2926.
57. Meier, A. E., Whittaker, M. M., and Whittaker, J. W. (1996) *Biochemistry 35*, 348−360.

BI010637A